Three-dimensional object texturing for visible-thermal fringe projection profilometers

Rigoberto Juarez-Salazar[a], Eberto Benjumea[b], Andres G. Marrugo[b], and Victor H. Diaz-Ramirez[c]

[a]CONAHCYT – Instituto Politécnico Nacional - CITEDI, Av. Instituto Politécnico Nacional 1310, Nueva Tijuana, Tijuana, B.C., 22435, México
[b]Facultad de Ingeniería, Universidad Tecnológica de Bolívar, Cartagena, Colombia
[c]Instituto Politécnico Nacional - CITEDI, Av. Instituto Politécnico Nacional 1310, Nueva Tijuana, Tijuana, B.C., 22435, México

ABSTRACT

Conventional fringe projection profilometers utilize cameras and projectors in the visible spectrum. Nevertheless, some applications require profilometers with a complementary thermal camera for the infrared spectrum. Since the point cloud is computed from pixel correspondences between the visible camera-projector pair, the texture in the visible spectrum is obtained by direct association of color from each image pixel to its corresponding point in the cloud. Unfortunately, the texture from the thermal camera is not straightforward because of the inexistence of pixel-point correspondences. In this paper, a simple interpolation-based method for determining the texture of the reconstructed objects is proposed. The theoretical principles are reviewed, and an experimental verification is conducted using a visible-thermal fringe projection profilometer. This work provides a helpful framework for three-dimensional data fusion for advanced multi-modal profilometers.

Keywords: Thermal imaging, Optical profilometry, Fringe projection, Distorted pinhole model.

1. INTRODUCTION

Fringe projection profilometry has become relevant in medical applications because of its contactless and high-precision features.[1] Conventional fringe projection profilometers employ a camera-projector pair in the visible spectrum to obtain the object's three-dimensional (3D) shape,[2] as shown in Fig. 1(a). A color 3D reconstruction can be obtained by assigning the pixels of a color image captured by the camera to the corresponding point in the cloud, as shown in Fig. 1(b). However, some medical studies also observe temperature distributions as a sign of biological activity.[3] Therefore, the profilometer must also include a thermal camera to acquire temperature images, as shown in Fig. 1(c). Unfortunately, unlike the color image, the temperature image pixels are not in correspondence with the points of the 3D point cloud.

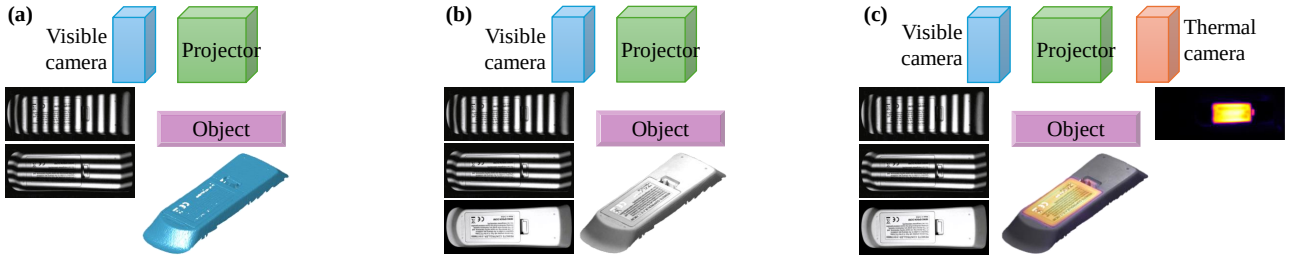

Figure 1. (a) Camera-projector pair performing 3D reconstruction by fringe projection in the visible spectrum. (b) Color 3D reconstruction using an additional color image captured by the visible camera. (c) Thermal 3D reconstruction by adding a temperature image captured by an incorporated thermal camera.

Further author information: (Send correspondence to R. Juarez-Salazar)
R. Juarez-Salazar: E-mail: rjuarezsa@conahcyt.mx, Telephone: +52 664 623 1344

Optics and Photonics for Information Processing XVIII, edited by Khan M. Iftekharuddin, Abdul A. S. Awwal, Victor Hugo Diaz-Ramirez, Andrés Márquez, Proc. of SPIE Vol. 13136, 131360E
 · 0277-786X · doi: 10.1117/12.3028321

In this paper, we propose a simple method for thermal 3D reconstruction using a conventional fringe projection profilometer equipped with a thermal camera. The distorted pinhole model is employed to deal with the high lens distortion exhibited by standard thermal cameras. The theoretical principles of the proposed method are given, and an experimental thermal 3D reconstruction validates its usefulness. The obtained results confirm the simplicity and efficiency of the proposed method in assigning thermal images to a 3D point cloud.

2. THEORY

2.1 Imaging process of cameras or projectors

In this work, the distorted pinhole model is regarded because of its simplicity and good performance against lens distortion. Since the generalization from the pinhole to the distorted pinhole model is straightforward,[4] the theoretical analysis will be conducted using the pinhole model for simplicity. The imaging process can be modeled as the computation of the image (or slide) point $\boldsymbol{s}$ where a point $\boldsymbol{p}$ of the 3D space was detected (or illuminated) as

$$\boldsymbol{s} = \mathcal{H}^{-1}[C\mathcal{H}[\boldsymbol{p}]], \tag{1}$$

where $\mathcal{H}$ is the homogeneous coordinates operator,[5] $C = K[R^T, -R^T\boldsymbol{t}]$ is the matrix of the device, K is the intrinsic parameter matrix, R and $\boldsymbol{t}$ are the rotation matrix and translation vector defining the pose of the device. Equation (1) can be inverted as

$$\boldsymbol{p} = \boldsymbol{t} + \lambda RK^{-1}[\boldsymbol{s}], \tag{2}$$

where λ is an unknown scalar, which parametrizes a straight line in the 3D space passing through $\boldsymbol{t}$ and having direction $RK^{-1}[\boldsymbol{s}]$.

2.2 Point correspondences, fringe projection, and triangulation

Three-dimensional object reconstruction by optical profilometry depends on point correspondences between a camera and a projector. Let C_c and C_p be the matrices of the camera and projector in the visible spectrum, respectively. Then, any point $\boldsymbol{p}$ in the field of view of both devices will be illuminated by the pixel $\boldsymbol{s}_p$ from the projector slide, and captured by the pixel $\boldsymbol{s}_c$ on the camera image as

$$\begin{aligned} \boldsymbol{s}_c &= \mathcal{H}^{-1}[C_c\mathcal{H}[\boldsymbol{p}]], \\ \boldsymbol{s}_p &= \mathcal{H}^{-1}[C_p\mathcal{H}[\boldsymbol{p}]]. \end{aligned} \tag{3}$$

Several alternatives exist to obtain point correspondences $\boldsymbol{s}_c \leftrightarrow \boldsymbol{s}_p$ in optical profilometry.[2] One of the most accurate and robust is fringe projection.[6] Fringe projection works as a communication system in which the projector transmits its pixel coordinates as a fringe pattern, and the camera receives and recovers the projector coordinates by phase demodulation.[7] Given a point correspondence $\boldsymbol{s}_c \leftrightarrow \boldsymbol{s}_p$, Eq. (2) can be employed to obtain the lines associated with the points $\boldsymbol{s}_c$ and $\boldsymbol{s}_p$ and determine the 3D point $\boldsymbol{p}$ as the intersection point (or minimum distance) between the lines.[8]

2.3 Three-dimensional object texturing

The triangulation process returns a cloud of points representing the reconstructed 3D object. However, the texture brought by the color on the object's surface is not present, as shown in Fig. 1(a). However, the visible camera (used to obtain point correspondences) can acquire an additional fringe-free photograph of the object under test, as shown in Fig. 1(b). In this way, the color recorded in a pixel $\boldsymbol{s}_c$ of the additional photograph is assigned to the point $\boldsymbol{p}$ in the reconstructed object. Unfortunately, this straight assignment is impossible if the texture comes from a camera other than that used for triangulation.

Let us suppose a thermal camera with matrix C_t is added to the fringe projection profilometer, as shown in Fig. 1(c). The thermal camera will register the temperature of the object at a point $\boldsymbol{q}$ on the pixel $\boldsymbol{s}_t$ as

$$\boldsymbol{s}_t = \mathcal{H}^{-1}[C_t\mathcal{H}[\boldsymbol{q}]]. \tag{4}$$

It is worth mentioning that although all devices are seeing the same object, the 3D points $\boldsymbol{q}$, captured by the thermal camera, and $\boldsymbol{p}$, triangulated by the visible camera-projector pair, are different. For this reason, the

temperature on a pixel $\boldsymbol{s}_t$ cannot be assigned to any point $\boldsymbol{p}$ of the reconstructed object. However, the thermal texturing can be performed by establishing point correspondences using interpolation as follows.

Let $T(\boldsymbol{s}_t)$ be the thermal image captured experimentally, and $\mathcal{T}(\boldsymbol{s})$ be an interpolant function fitted to $T(\boldsymbol{s}_t)$. The interpolant can be constructed using a convenient analytical function.[9] In particular, the two-dimensional linear polynomial works properly, although other more sophisticated interpolants, such as splines, can be used.[10] Next, all the points $\boldsymbol{p}$ obtained by triangulation are back-projected on the thermal camera as

$$\tilde{\boldsymbol{s}}_t = \mathcal{H}^{-1}[C_t \mathcal{H}[\boldsymbol{p}]]. \tag{5}$$

This step ensures a correspondence between every point $\boldsymbol{p}$ in the reconstructed object and its "pixel" $\tilde{\boldsymbol{s}}_t$ on the thermal image. Then, the temperature at the required point $\tilde{\boldsymbol{s}}_t$ is obtained using the interpolant function as

$$\tilde{T}(\tilde{\boldsymbol{s}}_t) = \mathcal{T}(\tilde{\boldsymbol{s}}_t). \tag{6}$$

Since $\tilde{\boldsymbol{s}}_t$ and $\boldsymbol{p}$ are in correspondence, the temperature $\tilde{T}$ can be assigned directly to $\boldsymbol{p}$ in the reconstructed 3D point cloud. The following section demonstrates the usefulness of the proposed approach experimentally.

3. EXPERIMENTAL EVALUATION

The proposed 3D object visible-thermal texturing method was evaluated experimentally by the setup shown in Fig. 2(a). The profilometer includes the visible camera iDS UI-3880CP-C-HQ, 3088×2076 pixels, the projector Kodak Luma 150, 1920×1080 pixels, and the Infiray thermal camera, 1296×870 pixels. The object under test was the bottom face of a remote control whose battery compartment cover was heated. Figure 2(b) shows the virtual representation of the experimental system using the estimated calibration parameters (intrinsic, extrinsic, and lens distortion).[11]

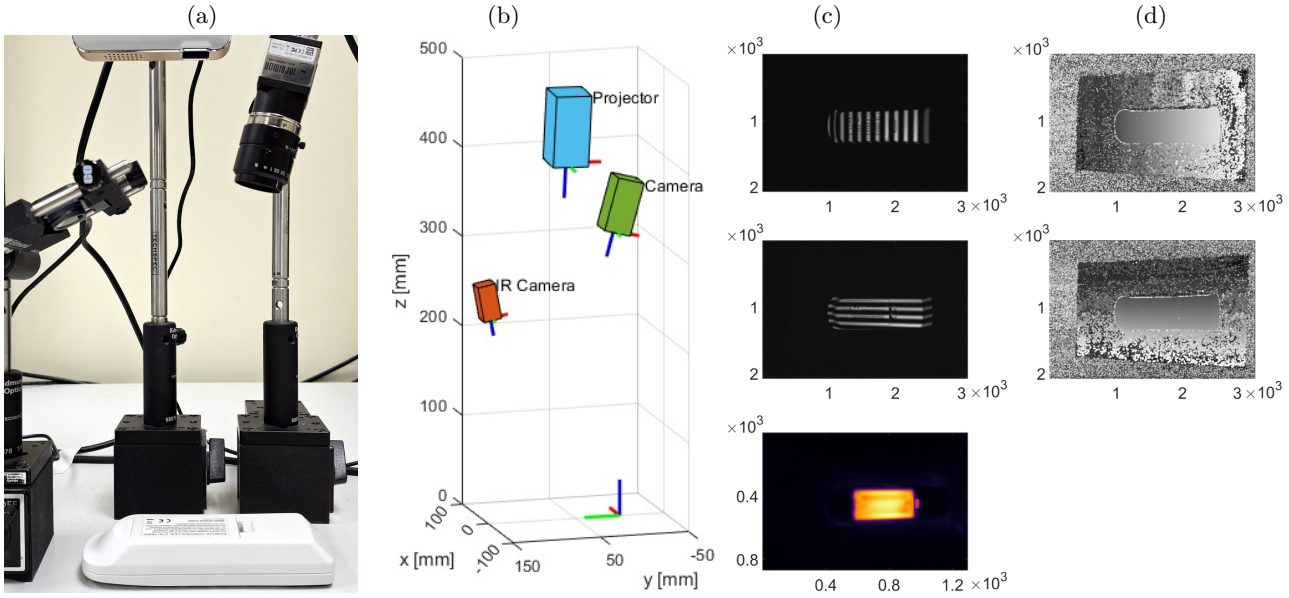

Figure 2. (a) Experimental visible-thermal fringe projection profilometer capturing the bottom face of a remote control whose battery cover was heated. (b) System representation using the estimated calibration parameters. (c) Two of forty-eight fringe patterns and the temperature map captured by the visible and thermal cameras, respectively. (d) Demodulated phase obtained by the multi-frequency phase shifting method.

The multi-frequency phase-shifting method was employed for phase demodulation.[7] Four gratings with different frequencies and six phase shifts were projected along the projector's x-axis (vertical) and y-axis (horizontal). Figure 2(c) shows one of the captured fringe patterns along the vertical and horizontal directions, respectively, and the temperature map captured by the thermal camera. Figure 2(d) shows the demodulated phases along the x- and y-axis obtained after processing the captured forty-eight fringe patterns.

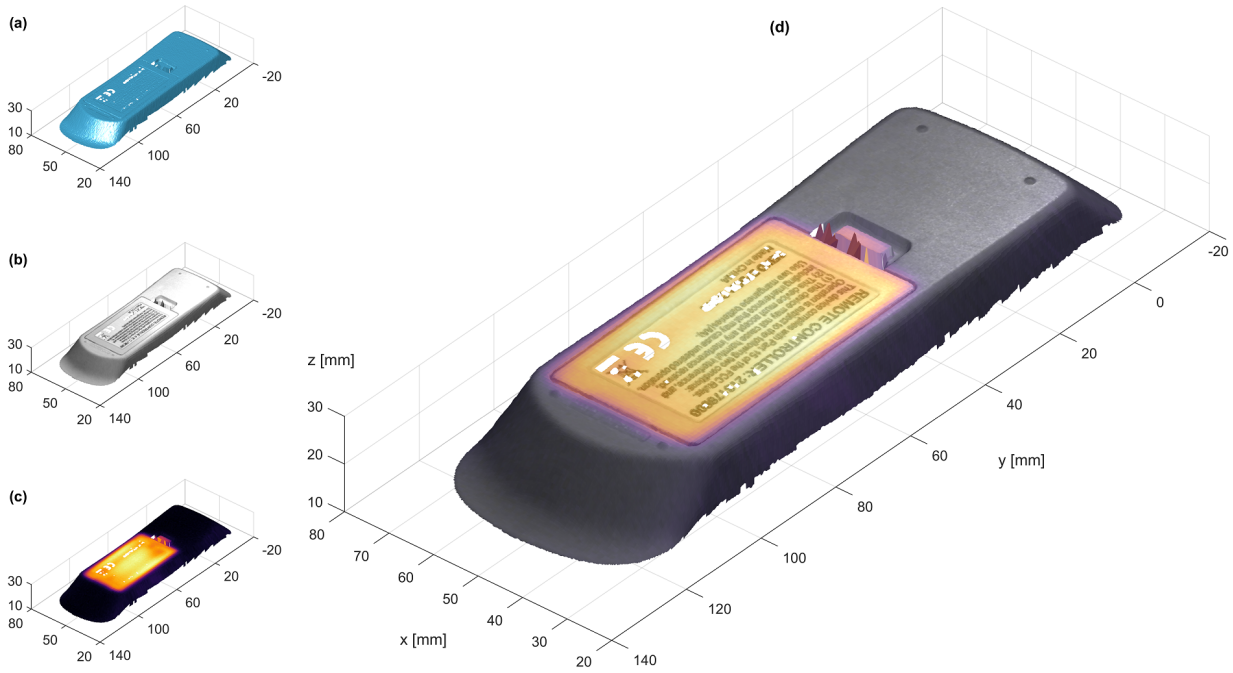

Figure 3. Three-dimensional object texturing results. (a) Point cloud of the reconstructed object. (b) Reconstruction with texture from the visible camera. (c) Reconstruction with texture from the thermal camera. (d) Visible-thermal texture by averaging the visible and thermal textures. Experimental images are available in Ref.[12]

Figure 3(a) shows the resultant 3D reconstruction obtained by triangulation using the parameters of the visible camera-projector pair and the demodulated phase.[8] The background light (fringe-free image), returned by the phase demodulation process, was used as the visible texture of the object. Figure 3(b) shows the result of assigning the background light to the corresponding points in the reconstructed object.

The temperature map $T(\boldsymbol{s}_t)$, shown in Fig. 2(c), was used to fit the interpolant function $\mathcal{T}(\boldsymbol{s})$ (two-dimensional linear polynomial). Next, the 3D point cloud was back-projected on the image plane of the thermal camera to obtain the corresponding "pixels" $\tilde{\boldsymbol{s}}_t$ by Eq. (5). Then, the interpolant function was evaluated at the points $\tilde{\boldsymbol{s}}_t$. Finally, the obtained temperature values were assigned to the reconstructed 3D object, as shown in Fig. 3(c). Both the visible and thermal textures were averaged to show them simultaneously on the reconstructed object, as shown in Fig. 3(d). It is worth mentioning that the described procedure is valid even though the imaging model is more sophisticated than the pinhole one. Particularly, in this work, the distorted pinhole model was employed to deal with the high lens distortion exhibited by thermal cameras. The implemented code is available online for further reference.[12]

4. CONCLUSIONS

A simple 3D object texturing for fringe projection profilometers equipped with a thermal camera was presented. The theoretical principles were described, and their usefulness was evaluated experimentally. The proposed approach's simplicity was shown to be independent of the employed imaging model. This feature is essential because some devices, such as thermal and fisheye cameras, could exhibit high distortion levels. The images and data employed for this study were made available online for implementation and testing. This work is a valuable complement to research on developing advanced multi-modal fringe projection profilometry.

ACKNOWLEDGMENTS

This work was supported by the Consejo Nacional de Humanidades, Ciencias y Tecnologías (CONAHCYT) by the projects Cátedras-880, and Basic Science and/or Frontier Science 320890. The authors thank the support of Instituto Politécnico Nacional by the project SIP-20240319.

REFERENCES

[1] Muyshondt, P. G., der Jeught, S. V., and Dirckx, J. J., "A calibrated 3d dual-barrel otoendoscope based on fringe-projection profilometry," *Optics and Lasers in Engineering* **149**, 106795 (2022).

[2] Geng, J., "Structured-light 3d surface imaging: a tutorial," *Adv. Opt. Photon.* **3**(2), 128–160 (2011).

[3] Ring, E., "The historical development of temperature measurement in medicine," *Infrared Physics & Technology* **49**(3), 297–301 (2007).

[4] Juarez-Salazar, R., Zheng, J., and Diaz-Ramirez, V. H., "Distorted pinhole camera modeling and calibration," *Applied Optics* **59**(36), 11310–11318 (2020).

[5] Juarez-Salazar, R. and Diaz-Ramirez, V. H., "Operator-based homogeneous coordinates: application in camera document scanning," *Optical Engineering* **56**(7), 070801 (2017).

[6] Zhang, S., [*High-Speed 3D Imaging with Digital Fringe Projection Techniques*], CRC Press, Boca Raton (2016).

[7] Juarez-Salazar, R., Giron, A., Zheng, J., and Diaz-Ramirez, V. H., "Key concepts for phase-to-coordinate conversion in fringe projection systems," *Applied Optics* **58**, 4828–4834 (jun 2019).

[8] Juarez-Salazar, R., Rodriguez-Reveles, G. A., Esquivel-Hernandez, S., and Diaz-Ramirez, V. H., "Three-dimensional spatial point computation in fringe projection profilometry," *Optics and Lasers in Engineering* **164**, 107482 (May 2023).

[9] Hamming, R., [*Numerical methods for scientists and engineers*], Dover Publications (2012).

[10] Chapra, S. C., [*Applied numerical methods with MATLAB for engineers and scientists*], McGraw-Hill (2018).

[11] Benjumea, E., Vargas, R., Juarez-Salazar, R., and Marrugo, A. G., "Toward a target-free calibration of a multimodal structured light and thermal imaging system," *Proceedings of SPIE* **13038**, 1303808 (2024).

[12] Juarez-Salazar, R., "3D Fringe Data Test: Thermal Texturing." User Fringe Pattern Data Base (Accessed: August, 2024) http://rjuarezs.com/s_3dfringe.html (August 2024).